High-frequency affine mechanics and nonaffine relaxation in a model cytoskeleton

David A. Head,[1] Emi Ikebe,[2] Akiko Nakamasu,[2] Peijuan Zhang,[2] Lara Gay Villaruz,[2] Suguru Kinoshita,[2] Shoji Ando,[3] and Daisuke Mizuno[2,*]

[1]*School of Computing, Leeds University, Leeds LS2 9JT, United Kingdom*

[2]*Department of Physics, Faculty of Exact Sciences, Kyushu University, Fukuoka 812-8581, Japan*

[3]*Faculty of Biotechnology and Life Science, Sojo University, Kumamoto 860-0082, Japan*

(Received 1 December 2011; revised manuscript received 25 February 2013; published 21 April 2014)

The cytoskeleton is a network of crosslinked, semiflexible filaments, and it has been suggested that it has properties of a glassy state. Here we employ optical-trap-based microrheology to apply forces to a model cytoskeleton and measure the high-bandwidth response at an anterior point. Simulating the highly nonlinear and anisotropic stress-strain propagation assuming affinity, we found that theoretical predictions for the quasistatic response of semiflexible polymers are only realized at high frequencies inaccessible to conventional rheometers. We give a theoretical basis for determining the frequency when both affinity and quasistaticity are valid, and we discuss with experimental evidence that the relaxations at lower frequencies can be characterized by the experimentally obtained nonaffinity parameter.

DOI: 10.1103/PhysRevE.89.042711 PACS number(s): 87.16.dm, 83.80.Lz, 83.85.Ei, 87.16.dj

I. INTRODUCTION

Most eukaryotic cells have their own mechanical framework or *cytoskeleton*, which is a composite of protein filaments such as actin, microtubules, and various intermediate filaments. The cytoskeleton performs a range of mechanical roles during cell division, migration, and contraction [1,2], by transmitting and responding to forces generated by molecular motors [3,4]. Quantitative and analytical mechanical response models have relied on the assumption of *affinity*, i.e., a self-similar strain field on all length scales, while theoretical efforts have predicted violation of this fundamental assumption for a range of disordered materials [5], including glasses, gels, and colloids, not to mention cytoskeletons. Quantifying nonaffinity is challenging for both theory and experiments, as it is coupled to the local disordered structure and thus sensitively depends on microscopic degrees of freedom. While the majority of investigations have thus far been performed numerically at zero frequency, predictions are usually not falsifiable with existing experimental methods.

Cells or cytoskeletons have been theoretically regarded as (1) networks of semiflexible polymers or (2) glassy systems, in order to interpret their mechanical behaviors. Each explains different experimental observations characteristic of cytoskeletons; i.e., the former explains the highly nonlinear stiffening under applied stress [6–8] and the latter the slow relaxations at low frequencies in linear response [9,10]. The experiments mentioned above were performed with conventional technologies of limited bandwidth and fitted to models by qualitative scaling. The theoretical prediction for the affine response of semiflexible networks, however, has been given in quantitative form as the sum response of the constituent polymers characterized by their persistence lengths and cross-linking distances [11].

Here, we carry out high-bandwidth passive microrheology [12–16] on vimentin networks reconstituted *in vitro* and observe the nonlinear mechanical response due to forces propagating from a local source applied by an optical tweezer. Since the applied force is constant, the gel becomes equilibrated and the fluctuation-dissipation theorem can be employed to deduce the viscoelasticity of the local environment from the thermal fluctuations of colloidal probes. Our experiments unequivocally demonstrate the anisotropic stiffening of the cytoskeletal network behind the applied force, with greater stiffening in the parallel direction. Quantitative agreement with the affine model of network of semiflexible polymer is obtained for the response in both directions, but only for the response faster than certain critical frequency ranging ∼10–1000 Hz, which separates the high-frequency power law and low-frequency elastic behavior of the network. We therefore argue that the failure of the affine model at lower frequencies is due to the presence of nonaffinity, which can be characterized by the ratio of affine and nonaffine elasticity. We show that this experimentally obtained factor successfully predicts the theoretically incalculable slow response, in this study, the zero-frequency changes in particle separation, without any adjustables.

II. MATERIALS AND METHODS

Vimentin is a member of the intermediate filament (IF) family of proteins and is mainly expressed in mesenchymal cells. As in most IF networks, vimentin fibers crosslink by themselves without crosslinking reagents and show significant stiffening under uniform shear without network rupture [6,8,17], presenting an ideal system to study cytoskeletal mechanics. Experiments were carried out using preparations of vimentin proteins based on a standard protocol [18–21]. Vimentin proteins in subunit buffer were centrifuged at 13 K rpm, 4 °C for 30 min and diluted into polymerization buffer (5 mM PIPES pH 7.0, 1.0 mM DTT, 270 mM NaCl, 0.75 mg/ml vimentin) with a small amount of polystyrene latex beads (Polysciences Inc., Polybeads, 2.0-μm diameter, ∼1/1200 times diluted from stock solution). Samples were loaded onto an ice-cooled glass chamber and polymerized overnight under the optical laser trapping equipment at 30 °C. Complete polymerization took several hours.

*mizuno@phys.kyushu-u.ac.jp

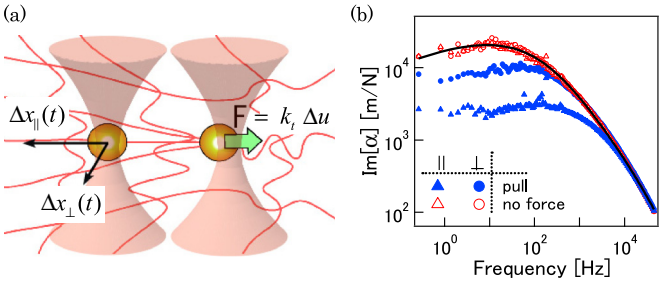

FIG. 1. (Color online) (a) Schematic of the experiment. A strongly trapped bead (right) was pulled away or pushed toward the probe particle (left). Note that actual network is much denser. (b) Imaginary part of the response function of a particle embedded in vimentin. Triangles and circles show parallel and perpendicular directions to the applied force, respectively. Filled symbols are under prestress and open symbols corresponds to zero force. The solid curve corresponds to the fit with Eq. (S9) in the Supplemental Materials [21].

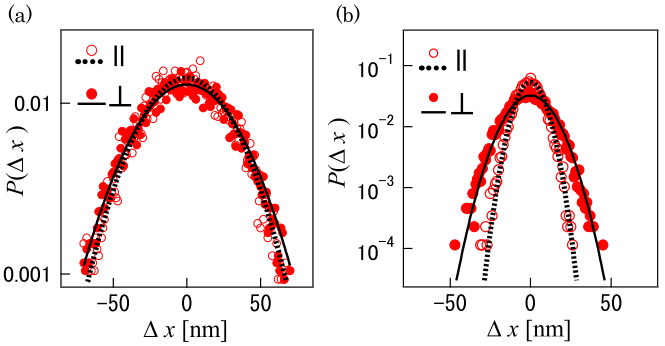

FIG. 2. (Color online) Van Hove distributions of the probe particle displacement for $\Delta t = 1$ s for (a) no force applied to the other bead $R \sim 8.5\ \mu$m away, and (b) the strongly trapped bead pulled away from the probe particle with an average force $F = 137$ pN. Displacements parallel (open circles) and perpendicular (closed circles) to the applied force, and their Gaussian fit (solid or broken line respectively), are shown. The widths ε of the Gaussian are 13.4 nm (parallel) and 19.7 nm (perpendicular).

Using dual-beam optical trapping microrheology, 2 polystyrene latex particles in the vimentin solution were weakly (∼0.75 mW) laser trapped at distances of $R \sim 8.5\ \mu$m in the same focal plane ($15 \sim 20\ \mu$m above the chamber bottom) immediately after sample preparation. After polymerization, one of the embedded beads was strongly trapped with a high-power NIR laser ($NdYVO_4$, 4W, $\lambda =$ 1064 nm, COMPASS, Coherent). By moving the piezo stage parallel to the line between the particles, a point force F up to 350 pN was locally applied to the vimentin network, generating an axisymmetric stress field [Fig. 1(a)]. Laser interferometry using quadrant photodiode detection [14] allows us to precisely measure the displacement of colloidal particles from the center position of the trapping laser [22,23]. Note that beads are much larger than the network mesh size and thus stably trapped. The other probe particle was weakly optically trapped by a semiconductor laser (CW 150 mW, $\lambda = 830$ nm, IQ1C150, Power Technology). The position fluctuations in orthogonal directions $\Delta x_\parallel(t)$ and $\Delta x_\perp(t)$ of this probe particle [Fig. 1(a)] were tracked by using another quadrant photodiode, and the output was sampled at 100 kHz by a 24-bit data acquisition board (PCI-4472, National Instruments). The response functions in parallel and perpendicular directions, $\alpha_\parallel$ and $\alpha_\perp$, respectively, were extracted from the spectra of the corresponding displacement spectra. Although the exact shear modulus is determined as 4-rank tensor [24], for convenience, we introduce "apparent" shear moduli based on the Stokes relation,

$$G_{\parallel(\perp)}(\omega) = 1/6\pi\alpha_{\parallel(\perp)}a, \tag{1}$$

where a is the particle radius. Details are given in Supplemental Material S1 [21].

III. RESULTS AND DISCUSSIONS

First, we directly observed the fluctuation of the probe particle by taking microscope images (30 Hz sampling for 60 s, $n = 5$) and calculated the van Hove correlation function $P(\Delta x), \Delta x(\Delta t) = x(t_0 + \Delta t) - x(t_0)$ to obtain the distribution of the probe particle displacements for $\Delta t = 1$ s (Fig. 2). Results were fitted to a Gauss function $f(\Delta x) = B\exp[-(\Delta x/\varepsilon)^2]$. As shown in Fig. 2(a), the thermal fluctuations of the probe particle are evidently isotropic if the force is not applied. When the strongly trapped particle (∼90 mW laser power, and $k_t \sim 1.4 \times 10^{-4}$ N/m trap stiffness) was pulled away from the probe particle, the fluctuations of the probe particle in the parallel direction were clearly suppressed relative to the perpendicular direction as shown in Fig. 2(b). To precisely investigate this anisotropy, we measured the frequency-dependent response functions of the probe particle embedded in the uniaxially stressed vimentin network with laser interferometry and analyzed the data as explained above. Im[$\alpha_\parallel$] was clearly smaller than that for zero force at low frequencies; see Fig. 1(b). Im[$\alpha_\perp$] was also reduced, but by a markedly smaller degree than Im[$\alpha_\parallel$]. As a control, we repeated the experiments in PAAm gel, a crosslinked network consisting of synthetic, flexible polymers. As demonstrated in Fig. S1 [21], no significant stiffening or anisotropy was detected.

We hypothesize that both the nonlinearity and anisotropy are primarily due to the stiffening of vimentin filaments under tension. The nonlinear force-extension relation of individual filaments has also been evoked to explain the macroscopic, uniform response of cytoskeletal gels [6,7]. Filaments aligned parallel to the line of force will be placed in a state of greater tension and thus become stiffer than those orthogonally aligned, resulting in the observed anisotropic response. Quantitative estimates for networks of fibers obeying the wormlike chain model can be made once two key assumptions are adopted: that the network response can be treated as affine, and that geometrical nonlinearities such as filament rotation are negligible. Then the static prestress and strain distribution around the applied point force and the differential responses $\alpha_{\parallel(\perp)}$ are numerically calculated if three material parameters are given: persistence length ℓ_p, length density of filaments ρ, and crosslinking distance ℓ_c. Details of the calculation are described in full elsewhere [24]. Before we present results of this procedure, we first examine the validity for the assumption of affinity for vimentin networks.

Many theoretical studies have suggested that the static response of semiflexible networks frequently exhibits nonaffinity when they are crosslinked with filaments less than Maxwell's isostatic connectivity per each node [25,26]. Due to the static situation, all these studies do not take the solvent response into account. For the dynamic response at high frequencies, however, the motion of network and solvent is strongly coupled so that the gel behaves as a single incompressible continuum, ensuring the affinity. We therefore believe that semiflexible polymer networks often deform nonaffinely to a degree that depends on frequency: High-frequency perturbations invoke an affine response, which becomes increasingly nonaffine as the frequency is lowered [28]. When affinity can be assumed, the network response is proportional to that of a single-filament, which is the sum over modes with characteristic relaxation frequency $\propto\lambda^{-4}$ for wavelengths λ not exceeding ℓ_c [11]. This leads to a high-frequency power law $G(\omega) \propto (-i\omega)^{3/4}$ [so $G'(\omega) < G''(\omega)$] above $\omega_1 \propto \kappa/(\zeta \ell_c^4)$ with $\kappa = \ell_p k_B T$ the filament bending modulus and ζ the drag coefficient [11], where ω_1 is the relaxation frequency for the longest wavelength fluctuations between crosslinks. This power-law behavior has been observed for crosslinked cytoskeletons when the effects of inertia and solvent viscosity can be neglected or corrected [14,21,23,29]. The prefactor for this power law is insensitive to the crosslinking distance ℓ_c and depends only on the known parameters ρ, ζ, the bead radius a, and the unknown persistence length ℓ_p. The solid curve in Fig. 1(b) shows the fit carried out by assuming $G(\omega) = A + B(-i\omega)^a + C(-i\omega)^{0.75} - i\omega\eta_0$, where $\eta_0 = 0.00089$ Pa s is the viscosity of the solvent; see Supplemental Materials S4 for details [21]. The fit clearly supports the 3/4 power law for the high-frequency response. We therefore obtain $\ell_p \approx 0.8$ μm for our vimentin networks.

Let us suppose that the network continues to deform affinely below ω_1. Then fluctuation modes with wavelengths larger than ℓ_c do not exist, and the network exhibits an elastic plateau $G'(\omega) \approx G_0 > G''(\omega)$ [11]; see solid curves in Fig. 3(a). The crossover frequency ω_1 can then be extracted from experimental data as the point where $G'(\omega_1) \approx G''(\omega_1)$. As shown in Figs. 3(a) and 3(b), the expected $\sim\omega^{3/4}$ scaling at high frequencies is observed for $G''(\omega)$. Slight deviation is due to the inertia and the effect of the solvent viscosity. $G'(\omega)$ should also follow the similar power law, but only at higher frequencies than those shown, where the effects of inertia are not negligible and significant errors arising from the finite-bandwidth sampling hinder its correction [21]. The broken curves in Fig. 3(a) are the estimates not influenced by the error since they are calculated based on the fit shown in Fig. 1(b). It can be seen that the crossover frequency ω_1, which is no more than a kHz for all samples, is well-defined, and the data around the frequency is hardly affected by the error due to the finite bandwidth. It does not herald the onset of the predicted plateau, though; rather a slow decay is observed to much lower frequencies.

It is to be noted that the probe particle under $\approx$pN force application does not flow in our experimental time window; the dissociation of crosslinks, for instance, can be neglected. We therefore propose this is primarily due to *nonaffine* modes. At frequencies below ω_1, with the emergence of collective modes

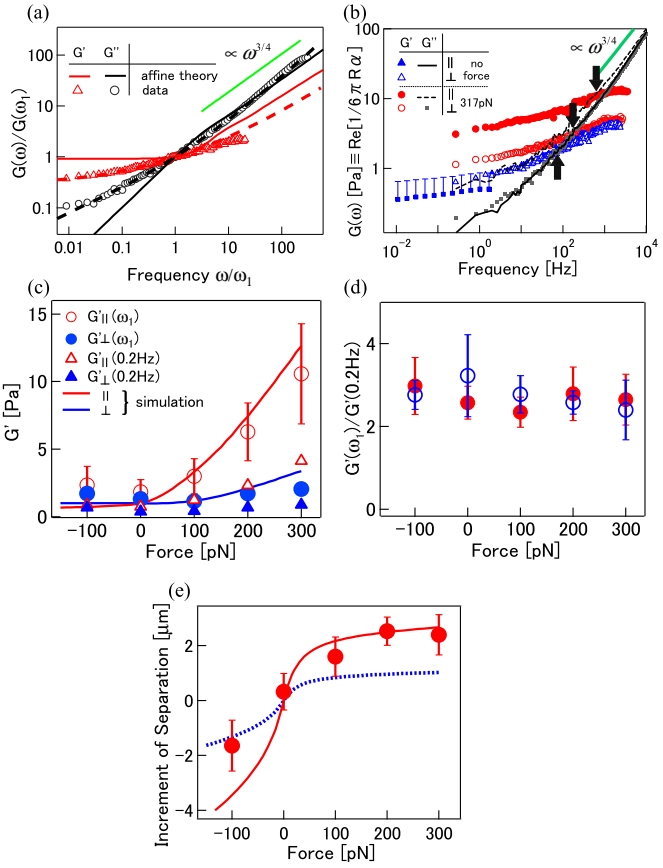

FIG. 3. (Color online) (a) Affine viscoelastic response of a crosslinked semiflexible network (solid curves) [11]. The high-frequency scaling $\sim\omega^{3/4}$ is shown as a solid line segment. Open circles and triangles are the scaled data without prestress. Broken curves are the expected behavior when the error due to the finite sampling is removed [21]. (b) Applied force dependence of $G'(\omega)$ [calculated using Eq. (1)] in parallel (closed symbols) and perpendicular (open symbols). The line segment at high frequencies show the power law [$\propto (-i\omega)^{3/4}$]. Filled squares with error bars show slow static response obtained with video microscopy without prestress. The gray dots and the broken line show $G''(\omega)$ under force application ($F = 317$ pN). The solid curve shows $G''(\omega)$ without prestress (averaged for both directions). The intersections with $G'(\omega)$ as shown by the arrows give $G'(\omega_1)$. (c) Dependence of $G'(\omega_1)$ (circles) and $G'(0.2\,\text{Hz})$ (triangles) with the force applied to the trapped bead ($n = 12$). Open and closed symbols correspond to parallel and perpendicular directions, respectively. Forces ranging from -150 to 350 pN were binned every 100 pN, with the median and standard deviation plotted (more negative forces gave irreproducible data). The smooth curves are the theoretical fit from Ref. [24] with $\ell_p = 0.8$ μm, $\ell_c = 0.6\,\mu$m, and $\rho = 16.25$ μm^{-2}. (d) Ratio of G' at ω_1 and 0.2 Hz for parallel (closed circles) and perpendicular (open circles) directions. (e) Change in probe separation induced by the force (circles) and the corresponding affine prediction for the same parameters as (c) (dashed line). The solid line gives the scaled prediction for nonaffine response.

with wavelengths longer than ℓ_c, the network can redistribute the deformations (thus energy cost) of each filaments in order to lower the total strain energy; i.e., it will be nonaffine. Here it is to be noted that the crossover frequency for the coupling-decoupling behavior between solvent and network is

length-scale r dependent as $\omega_c \sim G_0 l_c^2/\eta r^2$ [14], where η is the solvent viscosity and G_0 is the static network elasticity when affinity assumed. Since $\omega_1 \sim \omega_c$ for the length scale of the filaments $r \sim \ell_c$, these slow modes are decoupled from the solvent: the slower the frequency is, the larger the region of the nearby network that must reconfigure to give a mutually optimal configuration, independently of the surrounding solvent. This can be regarded as a *collective* problem in that there is only one optimal configuration for the local network, as expected for a disordered system such as this. As the frequency is lowered, the size of the mutually relaxing region increases. The region of configuration space that must be explored to find the optimum also expands, correspondingly increasing the time to reach equilibrium. This collective process explains the slow decay of viscoelasticity below ω_1 as observed. It is therefore at this crossover frequency ω_1, which lies near the high-frequency limit of the elastic, nonaffine regime, and the low-frequency limit of the viscous, affine regime, that we can compare the data to the affine mechanical model (which, by its nature, can only be used to predict the plateau modulus [24]).

The microrheology protocol employed here permits the extraction of three independent quantities for each applied force: the frequency-dependent shear moduli in parallel $G'_\parallel(\omega)$ and perpendicular $G'_\perp(\omega)$ directions measured at the probe, and the change in the particle separation. For $G'_\parallel$ and $G'_\perp$, we find good agreement with the theory of [24] at the crossover frequency ω_1 extracted from the curves, as shown in Fig. 3(c). Here we estimated $\rho \approx 16.25\ \mu\text{m}^{-2}$ from [30] and $\ell_p \approx 0.8\ \mu$m from the high-frequency data without prestress, leaving the single fitting parameter ℓ_c. We extract $\ell_c \approx 0.6\ \mu$m from the fit, consistent with previous estimates of vimentin networks formed following the same protocol [17]. It is to be noted that not any value of ℓ_c could fit the stiffening behavior of $G'_\parallel(0.2\text{ Hz})$ and $G'_\perp(0.2\text{ Hz})$ as partially shown in Fig. S2 [21]. For the affine theory, the static shear modulus without prestress is given as $G_0 = 6\rho k_B T l_p^2/\ell_c^3$ [11]. If nonaffine relaxations were not assumed, ℓ_c estimated from static elasticity $G_0 \sim G'(0.2\text{ Hz})$ would be smaller than that estimated from $G'(\omega_1)$. The affine model predicts that the prestress stiffening behavior is collapsed to a single universal curve using the force scaled as $Fl_c^2/\rho\ell_p R^2 k_B$T [24]. Larger ℓ_c therefore means more pronounced stiffening than experimentally observed, as shown in Fig. S2 [21].

The validity of the affine assumption at ω_1 must still be examined, since the prestress is realized under nonaffine network deformations. Interestingly, the ratio of $G'(\omega_1)$ to the plateau value appears to be independent of the applied force, as shown in Fig. 3(d). This insensitivity of strength of nonaffine relaxation $G'(\omega_1)/G'(0.2\text{ Hz})$ to the stiffening of the filaments has not, to the best of our knowledge, been predicted in any model, to which we give qualitative speculation here. The elastic energy of the network composed of semiflexible polymers involves the contributions from bending and entropic stretching deformations of constituent filaments and it is known that ℓ_p is the parameter for determining both [7,11]. The network condition $\ell_c \sim \ell_p$ of our vimentin sample is, however, out of the scope of previous theoretical studies on nonaffinity, where $\ell_c \ll \ell_p$ or $\ell_c \gg \ell_p$ is assumed [25–27]. For $\ell_c \sim \ell_p$, since there exists sufficient thermal bending fluctuations between crosslinks, the total bending energy is not sensitive to deformation modes longer than ℓ_c, which is nonaffine; only the energy cost originating from the entropic stretch of each filament matters for the nonaffine relaxations. In such cases, quantities less dependent on ℓ_p, such as the geometry of network connections and/or topological constraints due to the steric hindrance for the overlapping of filaments, play a more important role [31] for determining the strength of nonaffine relaxations; $G'(\omega_1)/G'(0.2\text{ Hz})$ is therefore independent of ℓ_p or the prestress stiffening of the network. Regardless of the theoretical interpretation, this experimental finding $G'(\omega_1)/G'(0.2\text{ Hz}) \approx 2.6$ indicates that affine estimations valid at ω_1 can be directly extended to the zero-frequency for prestress distributions, by the simple application of a constant scaling factor of $\approx$2.6 for prestrain distributions.

The affine model is not expected to fit the particle separation data, as this was measured at zero-frequency for which nonaffinity is present, and indeed the afffine model underestimates the separations as shown in Fig. 3(e). However, applying the constant factor $G'(\omega_1)/G'(0.2\text{ Hz}) \approx 2.6$ allows us to estimate the prestrain distributions, including nonaffinity as explained in the previous paragraph and that leads to agreement with experiments as shown in the figure. We conclude that all of our experimental data is consistent with nonlinear filament stiffening in a network that deforms increasingly nonaffinely as the frequency is decreased, and expect future experimental or theoretical studies to directly quantify this phenomenon will confirm our hypothesis. Note that the deviation for large pushing forces in Fig. 3(e) is due to the close approach of the beads, violating the point-particle assumption of the model.

In typical cell situations, the function of many receptors or protein catalysts can be modulated by the action of the forces transmitted via the cytoskeleton. This in turn influences signal transduction, biochemical reactions, and cell behavior. Our findings present a unique possibility to quantify the stresses spontaneously generated in the cell, by analyzing the affine response at frequency ω_1. Such frequencies are only accessible to high-bandwidth techniques such as microrheology, since $2\pi\omega_1 \sim$ 100–1000 Hz for typical cross-linked cytoskeletons. Indeed, the nonaffine elasticity measured at low frequencies with macrorheometry may tend to slightly underestimate filament bending stiffness [17,32], compared to the direct estimates from single filaments [33,34].

IV. CONCLUSION

We have demonstrated that the static strain exhibited in the model cytoskeleton can be quantitatively and consistently interpreted as a consequence of relaxation from the high-frequency affine response to the low-frequency nonaffine behavior. The frequency separating these two response regimes lies close to the crossover frequency ω_1 predicted from affine network theory, and it is around this frequency that our affine, mechanical model applies. Many soft condensed materials such as gels, glasses, and colloids also show high-frequency power-law behavior and slow relaxation. The theoretical basis for determining the critical frequency ω_1 and relating each

frequency range for affine and nonaffine response may also be applicable for these materials. The combination of high-bandwidth microrheology with a theoretical affine response model is uniquely placed to experimentally characterize the exotic slow nonaffine response, which remains elusive despite its ubiquitous importance for a vast range of materials.

ACKNOWLEDGMENTS

We thank F. MacKintosh, C. F. Schmidt, and S. Koster for helpful discussions. This work was supported by KAKENHI Grants No. 2510311, No. 25127712, No. 23684036, and No. 24657105 and the Asahi Glass Foundation.

[1] T. D. Pollard, D. Vavylonis, J. Q. Wu, S. Hao, and B. O'Shaughnessy, Science **319**, 97 (2008).
[2] S. L. Moores, J. H. Sabry, and J. A. Spudich, Proc. Natl Acad. Sci. USA **93**, 443 (1996).
[3] D. Mizuno, R. Bacabac, C. Tardin, D. Head, and C. F. Schmidt, Phys. Rev. Lett. **102**, 168102 (2009).
[4] D. Mizuno, C. Tardin, C. F. Schmidt, and F. C. MacKintosh, Science **315**, 370 (2007).
[5] S. Alexander, Phys. Rep. **296**, 65 (1998).
[6] C. Storm, J. J. Pastore, F. C. MacKintosh, T. C. Lubensky, and P. A. Janmey, Nature **435**, 191 (2005).
[7] M. L. Gardel, J. H. Shin, F. C. MacKintosh, L. Mahadevan, P. Matsudaira, and D. A. Weitz, Science **304**, 1301 (2004).
[8] P. A. Janmey, U. Euteneuer, P. Traub, and M. Schliwa, J. Cell Biol. **113**, 155 (1991).
[9] B. Fabry, G. N. Maksym, J. P. Butler, M. Glogauer, D. Navajas, and J. J. Fredberg, Phys. Rev. Lett. **87**, 148102 (2001).
[10] P. Bursac, G. Lenormand, B. Fabry, M. Oliver, D. A. Weitz, V. Viasnoff, J. P. Butler, and J. J. Fredberg, Nat. Mater. **4**, 557 (2005).
[11] F. Gittes and F. C. MacKintosh, Phys. Rev. E **58**, R1241 (1998).
[12] T. G. Mason and D. A. Weitz, Phys. Rev. Lett. **74**, 1250 (1995).
[13] F. Gittes, B. Schnurr, P. D. Olmsted, F. C. MacKintosh, and C. F. Schmidt, Phys. Rev. Lett. **79**, 3286 (1997).
[14] B. Schnurr, F. Gittes, F. C. MacKintosh, and C. F. Schmidt, Macromolecules **30**, 7781 (1997).
[15] T. G. Mason, K. Ganesan, J. H. van Zanten, D. Wirtz, and S. C. Kuo, Phys. Rev. Lett. **79**, 3282 (1997).
[16] J. C. Crocker, M. T. Valentine, E. R. Weeks, T. Gisler, P. D. Kaplan, A. G. Yodh, and D. A. Weitz, Phys. Rev. Lett. **85**, 888 (2000).
[17] Y. C. Lin, N. Y. Yao, C. P. Broedersz, H. Herrmann, F. C. MacKintosh, and D. A. Weitz, Phys. Rev. Lett. **104**, 058101 (2010).
[18] H. Herrmann, I. Hofmann, and W. W. Franke, J. Mol. Biol. **223**, 637 (1992).
[19] H. Herrmann, L. Kreplak, and U. Aebi, Intermed. Fil. Cytoskel. **78**, 3 (2004).
[20] S. Ando, R. Gohara, S. Nishikawa, and Y. Takasaki, J. Biochem. **144**, 675 (2008).
[21] See Supplemental Material at http://link.aps.org/supplemental/10.1103/PhysRevE.89.042711 for details on sample preparation, data extraction and fitting, and additional response curves.
[22] F. Gittes and C. F. Schmidt, Meth. Cell Biol. **55**, 129 (1998).
[23] D. Mizuno, D. A. Head, F. C. MacKintosh, and C. F. Schmidt, Macromolecules **41**, 7194 (2008).
[24] D. A. Head and D. Mizuno, Phys. Rev. E **88**, 022717 (2013).
[25] C. P. Broedersz, M. Sheinman, and F. C. MacKintosh, Phys. Rev. Lett. **108**, 078102 (2012).
[26] E. M. Huisman and T. C. Lubensky, Phys. Rev. Lett. **106**, 088301 (2011).
[27] M. Dennison, M. Sheinman, C. Storm, and F. C. MacKintosh, Phys. Rev. Lett. **111**, 095503 (2013).
[28] E. M. Huisman, C. Storm, and G. T. Barkema, Phys. Rev. E **82**, 061902 (2010).
[29] G. H. Koenderink, M. Atakhorrami, F. C. MacKintosh, and C. F. Schmidt, Phys. Rev. Lett. **96**, 138307 (2006).
[30] H. Herrmann, M. Haner, M. Brettel, N. O. Ku, and U. Aebi, J. Mol. Biol. **286**, 1403 (1999).
[31] M. Rubinstein and S. Panyukov, Macromolecules **35**, 6670 (2002).
[32] M. Schopferer, H. Bar, B. Hochstein, S. Sharma, N. Mucke, H. Herrmann, and N. Willenbacher, J. Mol. Biol. **388**, 133 (2009).
[33] S. Winheim, A. R. Hieb, M. Silbermann, E. M. Surmann, T. Wedig, H. Herrmann, J. Langowski, and N. Mucke, Plos One **6**, e19202 (2011).
[34] N. Mucke, L. Kreplak, R. Kirmse, T. Wedig, H. Herrmann, U. Aebi, and J. Langowski, J. Mol. Biol. **335**, 1241 (2004).